Journal of Materials Research and Technology 35 (2025) 1141–1156

Contents lists available at ScienceDirect

Journal of Materials Research and Technology

journal homepage: www.elsevier.com/locate/jmrt

Systematic approach to paired ceramic coatings deposited by oxygen fuel and metal in a tribological application

K.A. Habib [a,*], D.L. Cano [a], Emilo Rayón [b], J. Serrano-Mira [a], José V. Abellán-Nebot [a], I. Cervera [a]

[a] Department of Industrial System Engineering and Design, Universitat Jaume I, 12071, Castellón, Spain
[b] Institut de Tecnologia de Materials, Universitat Politécnica de Valéncia, Camino de Vera, S/N-46022, Valencia, Spain

ARTICLE INFO

Handling editor: M Meyers

Keywords:
Al_2O_3–TiO_2
OF coatings
Metallic disc
Work-hardening
Stribeck curve

ABSTRACT

This study investigated nanostructured Al_2O_3 and Al_2O_3–TiO_2 composite coatings (e.g., 3, 13 and 40% TiO_2, mass fraction) deposited by the oxygen fuel (OF) spraying technique. The coatings exhibited varying hardness values, ranging from 705 $HV_{0.2}$ for Al_2O_3-40%T to 1317.9 $HV_{0.2}$ for Al_2O_3. To compare the behaviours of the coated specimens, the mechanical properties and effects of hardness ratio on the lubrication regimes were studied using the Stribeck curve. The higher TiO_2 content contained in the Al_2O_3–TiO_2 coating system yielded relatively inferior mechanical properties but lower porosity (ranged between from 18.3% A to 0%T to 1.64% A-40%T) and initial and final hardness ratio (16.2% Al_2O_3 to 9.2% Al_2O_3–40%TiO_2). Microstructural and phase analyses showed that this finding can be attributed to the special phase, Al_2TiO_5, and to the pre-existing microcracks in the coating. Thus, Al_2O_3–13%TiO_2 exhibited better characteristics for mechanical applications and oil film stability as compared with pure Al_2O_3 and 3% and 40% TiO_2 coatings. This study provides a reference for the design of Al_2O_3–TiO_2 ceramics with good wear resistance and a minimal friction coefficient under lubrication conditions. The strain hardening produced on the surfaces of the worn discs and the hardness ratio determined the tribological properties of the friction pairs. In summary, this work analysed the friction and wear properties of four ceramic coatings and their counterpart metallic discs under lubrication conditions using Stribeck curve, to provide an experimental basis for screening optimal materials for the key friction and wear pairs of industrial design and applications. The proposed methodology may assist in predicting variations in lubrication regime parameters (Stribeck curve) by controlling the hardness ratio.

1. Introduction

Alumina-titania (Al_2O_3–TiO_2) composite coatings deposited by thermal spraying techniques are known for their high toughness, remarkable abrasive and sliding wear resistance, high melting point, good chemical stability, low density, low thermal expansion, and low thermal conductivity. These properties make Al_2O_3–TiO_2 composites desirable materials for construction and coatings for high-performance applications in which thermal barriers are required [1]. Al_2O_3–TiO_2 coatings are excellent candidates for providing protection against abrasive wear and are helpful in various tribological applications such as (include, namely); coating for machinery, oil, textile, chemical industries, sleeve shafts, thermocouple jackets, pump shafts and in any other solicitation where it is necessary to combine high resistance to wear, low friction coefficient and high surface temperature. They are also resistant to high-temperature erosion (depending on the TiO_2 content) with cryogenic compatibility, are widely applied in surface engineering, and have high resistance [2]. When TiO_2 is added to Al_2O_3, the wear and adhesion strength both increase, and the toughness of the coating improves without altering its hardness [3]. This improves coating performance.

Industrial thermal spraying is a well-established method for enhancing tribological performance and corrosion resistance, thereby extending the lifespan of machine components [4–7]. Coatings deposited using the thermal spray process are created through multiple passes of successive spray droplet impacts in fully and/or partially molten states, followed by their flattening, rapid cooling, and solidification. Al_2O_3–TiO_2 coatings are usually deposited using plasma spray (PS) techniques. This is because a high working temperature is necessary to melt the ceramic feedstock particles, whereas a lower proportion of melt

* Corresponding author.
E-mail address: razzaq@esid.uji.es (K.A. Habib).

https://doi.org/10.1016/j.jmrt.2025.01.099
Received 17 December 2024; Received in revised form 9 January 2025; Accepted 13 January 2025
Available online 14 January 2025

particles or smaller particles are often found when the high-velocity oxygen fuel (HVOF) process is used [8,9].

Oxygen fuel (OF) is a versatile coating process that can be used to deposit a wide range of materials, including metals, ceramics, polymers, and their composites. In this process, the feedstock powder is introduced into a high-velocity and high-temperature OF flame generated by the combustion of the process gas (C_2H_2, O_2, and compressed air). The feedstock powder is deliberately completely melted or semi-melted during flight and re-solidified as it impacts the substrate surface, forming a sputter-like structure. The quality of a surface workpiece significantly affects its service life, wear resistance, fatigue resistance, atmospheric and high-temperature oxidation, and corrosion resistance.

OF has been applied to several essential products and components in the steel manufacturing, semiconductor, automobile, defense, and aerospace industries [10–12].

As a representative engineering ceramic material, Al_2O_3 is affordable, readily available, and has high strength, wear resistance, insulation properties (thermal and electrical), and chemical stability, which have promoted its widespread use in numerous applications. The high melting-point temperature of these coatings makes them more difficult to cast, and poor machinability induced by brittleness hinders the processing of materials. Through OF, a thick Al_2O_3 coating of approximately several hundred microns can be deposited at a high deposition rate and relatively low substrate temperature and under normal atmospheric conditions. Because of these industrial advantages, several studies have focused on the deposition of Al_2O_3-based OF, PS, and HVOF coatings in terms of their microstructures and properties. Other studies have investigated thermally sprayed Al_2O_3–TiO_2 systems [13–18]. One study reported that the addition of TiO_2 to the Al_2O_3 coating could affect the coating quality, particularly its mechanical and corrosion properties, including its hardness and toughness [8]. Other studies have examined the impact of the number of layers and sintering temperature on the microstructure, wear resistance, and corrosion resistance of Al_2O_3–TiO_2 multilayer coatings deposited on AISI 316L plates using the sol-gel dip coating technique [19]. The results indicated that an increase in the TiO_2 content deteriorates hardness but is beneficial for toughness.

Friction under lubricating conditions varies significantly depending on the corresponding lubrication regimes. The Stribeck curve illustrates the relationship between the coefficient of friction and the lubrication parameter or Hersey number (viscosity × speed/load). This curve classifieds the lubrication regimes into boundary, mixed, and hydrodynamic (fluid film) lubrication. In recent years, enhanced tribological performance, mechanical, wear mechanism as well as tribochemistry of the fabricated NiAl/Nb/Ag coatings have been reported, leading to a growing interest in the study and analysis of this type of coatings [20, 21].

Due to the excellent hardness and toughness of Al_2O_3–TiO_2 ceramic coatings, they are suitable for various tribological applications. Extensive research has been conducted on the wear resistance of Al_2O_3–TiO_2 coatings. However, prior studies on Al_2O_3–TiO_2 coatings deposited using thermal spray techniques do not sufficiently address the influence of the hardness ratio of friction pairs on lubrication regimes, as represented by the Stribeck curve, both before and after the friction process. Furthermore, these studies lack an analysis of how optimizing the hardness ratio of friction pairs and friction conditions affect lubrication regime changes during bulk metal forming, which involves a certain degree of plastic deformation of the counterpart metallic disc.

This study investigated and quantified the tribological behaviours of various ceramic coatings (i.e., nanostructured Al_2O_3-based and Al_2O_3–TiO_2 coatings) deposited using thermal spray techniques. These coatings were tested in contact with a hardened and tempered steel disc (F-5220) under different surface distress conditions and under varying combinations of surface hardness and hardness ratios. In this study, the surface hardnesses of the ceramic coatings remained constant following the tribological tests. Therefore, any differences in the surface hardening of the metallic counterpart steel disc caused by the ceramic coated pins could be attributed to the contact hardness ratio and coating microstructure. The second aim of this study was to assess experimentally the tribological behaviour (friction, wear losses and lubrication regime), work hardening of metallic discs, and friction coefficients of various Al_2O_3-based ceramic coatings with different TiO_2 contents. These assessments were performed under varying sliding friction conditions using pin-on-disc testing with a focus on comparing the performances of the different Al_2O_3 ceramic coatings under lubricated sliding conditions. The experimental data evidence for how the Stribeck curve changes if one surface in the contact is changed in hardness due to the working conditions. Test data were fitted with regression models. The fitted equations allow a robust assessment of the effect of the strain hardening on the counterpart disc and working conditions on the friction coefficient in components that operate in the lubrication conditions. Therefore, these equations may help to select the adequate coating and tribological performance for specific technological applications. A Stribeck curve was utilised to determine the effects of the hardness ratio on the lubrication regimes. This study offers insights into the design of Al_2O_3 and Al_2O_3–TiO_2 ceramic coatings (or/and any other friction pairs) with enhanced tribological performance, improved wear resistance, reduced friction, and increased efficiency. The study also attempts to optimise the hardness ratio for specific industrial tribological applications.

2. Experimental procedure

2.1. Materials and feedstock powder

Stainless steel AISI 304 was selected as the substrate material because of its excellent mechanical properties and resistance to high-temperature oxidation. The test samples consisted of rods with diameters of 8 mm and lengths of 18 mm. The chemical composition (in wt %) of the base metal substrate was 17.5–19.5% Cr, 8–10% Ni, 2% Mn, 1% Si, 0.11% N, 0.07% C, 0.05% P, and 0.03% S, where the rest of the composition was Fe. In this study, agglomerated nanostructured high-purity α-Al_2O_3-based (99.98%) ceramic coatings were deposited via the OF method using raw materials with different TiO_2 contents (0, 3, 13, and 40%). The feedstock for the OF process consisted of agglomerates formed from nanoparticles, as nanopowders cannot be directly fed into spray guns. The powder and coatings were designated as A-0%T (Al_2O_3), A-3%T (Al_2O_3-3% TiO_2), A-13%T (Al_2O_3-13% TiO_2), and A-40%T (Al_2O_3-40'% TiO_2), although the manufacturers of the used raw materials were different. Specifically, Ni–Al (Rototec 51000, Castolin Eutectic), operating as a bond coat, was applied to the substrate to improve the adhesion of the Al_2O_3-based topcoat (finishing layer) and to sustain thermal residual stress by utilising cyclic thermal loading, which improves the adhesion properties of the total coating system. Scanning electron microscopy (SEM) micrographs of the powders exhibited a near-spherical shape with an agglomerated surface. The particle size distribution was under a grain size of 13–40 μm. Fig. 1 shows the four distinct types of Spray-dried agglomerated nanostructured powders used in these experiments, which were ceramic finishing layers referenced as Nanox S2603S, S2613S, and S2640S with three different chemical compositions and nanostructured Al_2O_3 with 3, 13, and 40% TiO_2 feedstocks. The ceramic powders were purchased from Inframat Advanced Materials (USA).

2.2. Thermal spray procedure

Flame spraying of the bounding layer and four ceramic coating finishing layers (Al_2O_3, 3, 13, and 40% TiO_2) was performed using OF with a neutral flame of oxyacetylene CDS-8000 produced by Castolin Eutectic (Switzerland). The specimens were coated with Al_2O_3 and Al_2O_3–TiO_2 on one end of each AISI 304 pin. Table 1 lists the parameters of the thermal deposition process. Prior to the coating process, the surfaces of the specimens were cleaned by a grit-blasting gun using corundum

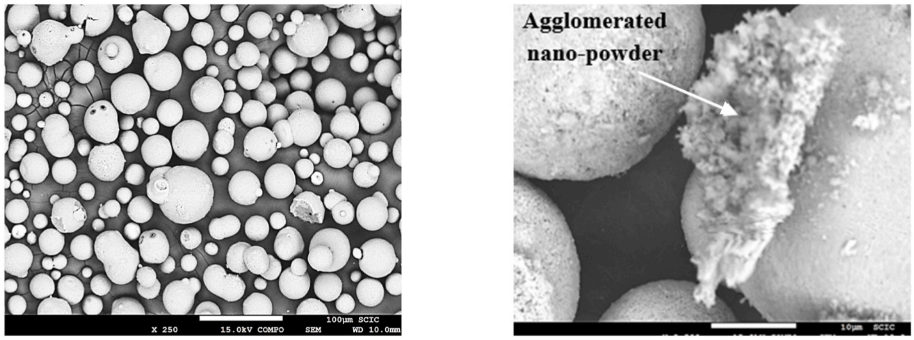

a)		b)

Fig. 1. SEM micrographs of spray-dried agglomerated nanostructured feedstock powders of Al_2O_3 and Al_2O_3–TiO_2 composite coatings with 3%, 13%, and 40% TiO_2 mass fractions: a) low magnification and b) magnified view.

Table 1
Thermal spray parameters.

Torch velocity (m/s)	Sprayed alloy	Preheating stroke Nº	Spray stroke Nº	Spraying distance (mm)	Compressed air pressure (bar)
67.5	Rototec	1	1	150	1.5
67.5	51000 A-0%T	0	6	85	3
67.5	A-3%T	0	6	85	3
67.5	A-13%T	0	6	85	3
67.5	A-40%T	0	6	85	3

particles of 99.6% purity and 36-mesh grit size at a distance of 0.2 m. The cleaning was conducted under an air pressure of 6 kg/cm^2 for nearly 1 min at an incident angle of approximately 45°. The purpose was to remove any possible surface oxides and create a surface roughness profile to ensure a strong bond between the deposited coating (bounding layer) and the substrate base metal. Prior to the tests, the ceramic coatings were ground and polished using a profilometer (Pethometer MI, Mahr GmbH, Germany) to maintain the R_a of the free surface below 2.0 ± 0.08 μm. The average thickness of the coating after thermal spraying was approximately 0.85 mm. The specimens were then ground and polished to obtain a ceramic coating of approximately 0.75 mm. Five measurements of the initial surface roughness (R_a) of the hardened and tempered disc F-5220 were conducted, and then the average and standard deviation were determined (1.79 ± 0.081 μm). The average surface roughness (R_a) of the deposited ceramic coating was 2.0 ± 0.08 μm. The mean roughness depth, defined as the vertical distance between the highest peak and deepest valley, was measured using a profilometer (Pethometer MI, Mahr GmbH, Germany) and determined to be 28.3 ± 2.4 μm.

2.3. Characterization of ceramic coatings

The microstructures of the alumina-based ceramics sprayed with OF on AISI 304 were investigated. Cross sections of the samples were mounted on resin and polished using conventional metallographic methods. These cross sections were prepared by epoxy mounting, grinding, and polishing with Al_2O_3 powder. The specimens were then cleaned in an ultrasonic bath at room temperature with acetone for 15 min and with distilled water. The specimens were then dried under hot-compressed air flow. The effects of TiO_2 on coating porosity were observed in the cross-sectional optical micrographs of the Al_2O_3-based coatings with different TiO_2 content (0, 3, 13, and 40%) in the deposited coating layers. The morphologies, compositions of the formed phases, and microstructures of the sprayed cross sections of a hot-mounted sample in epoxy resin were analysed by SEM (JOEL 7001F EDX-WDX Oxford) and energy-dispersive spectroscopy (EDS). The SEM cross sections of the coatings were analysed using Image-Pro Plus software to calculate the porosities of the different ceramic coatings.

The feedstock powders and deposited coatings were measured using X-ray diffractometry (XRD, D5000D by Siemens, Germany) with monochromatic Ni filtered Cu-Kα radiation at 20 mA and 35 kV to identify the crystalline phases. The scanning speed and goniometer range were 2°/min and 2°–70°, respectively. A SEM (IT-300, JEOL) equipped with EDS was used to characterise the microstructures of the coatings. The microhardness of the coatings was measured using an HMV Shimadzu microhardness tester according to ISO 6507 under an applied load of 200 gf ($HV_{0.2}$). The final Vickers microhardness value of the ceramic-deposited coatings was the mean of 10 random indentations.

The tribological properties of the four distinct types of top-finish-coat nanostructured Al_2O_3–TiO_2 ceramic coatings were investigated in a rotating unidirectional configuration using a TE79/P pin-on-disc multi-axis tribometer (Plint and Partners) under laboratory conditions. Ten drops/min of mineral oil (CUT-MAX 7–26 with viscosity = 3.2 ± 0.1 cSt at 40 °C and density = 0.820 g/cm^3 at 15 °C) were introduced to the contact area. Lower oil viscosity has been selected to highlight the effect of the hardness ratio of friction pairs on tribological behaviour. The other parameters used for testing were a relative sliding speed of 0.1 m/s, wear track radius of 36 mm, and a normal applied load of 20 N. Table 2 lists the wear-test parameters. The sliding speed was increased at each 75 m test run, and the mass loss was determined over a total sliding distance of 450 m. The wear loss (mg/s) of the ceramic pins was determined gravimetrically using a microbalance, and ultrasonic cleaning was performed on each of the pins. Three wear tests were performed for each type of ceramic coating, and the results were reproducible within 5%.

The pin-on-disk tests are preferably used to determine two-body sliding wear in lubrication conditions (after Stribeck curve). The pin is coated with the different ceramic material (A-0%T, A-3%T, A-13%T and A-40%T) that is slid against the metallic disk. The wear rates were calculated using the mean measurement value of steel disc in terms of the volume of the material removed per unit load and sliding distance, in unit of $mm^3 \cdot N^{-1}\ m^{-1}$. At least 5 wear tests were performed for

Table 2
Tribological tests parameters of the different friction pairs.

Parameters	Friction	Stribeck curve & wear
Load (N)	20	20
Truck radius (mm)	35	35
Sliding velocity (m/s)	0.07	0.04, 0.07, 0.11, 0.14, 0.18 and 0.21
Sliding time (s)	1800	1980
Distance (m)	252	450
Temperature (°C)	20	20
Relative humidity (%)	52	52

counterpart steel disc and their results were reproducible within 5 %. The counterpart disc used for the pin-on-disc tribology test in this study was made of hardened and tempered F-5220 steel (100 mm in diameter and 5 mm in thickness), in accordance with A68a (01), with an average microhardness of 930 HV_{200gf}. This choice aimed to emphasize the effect of ceramic coatings with varying hardness on the work hardening of the metallic disc while minimizing the potential for contrary effects.

3. Result and discussion

3.1. Microstructure study

Fig. 2 shows a cross-sectional SEM image at low magnification (x60) of the four samples (A-0, 3, 13, and 40% TiO_2), revealing the successful selection of thermally sprayed processing parameters for multilayered samples with distinct ceramic finish layers. The adherence between the bonding layer and ceramic finish layer was observed to be highly dependent on the TiO_2 content. This was because the melting point of TiO_2 (1843 °C) is less than that of Al_2O_3 (2072 °C). Thus, the melting degree of the feedstock was higher for higher TiO_2 content [22]. The average thickness of the Ni–Al bond layer was approximately 176 ± 14 μm, and the ceramic topcoat was approximately 879 ± 110 μm. A Ni-based bond coat was used to sustain the residual thermal stress and ensure the adhesion properties of the coating system. A cross-sectional overview of the Ni-based bonding layer shows highly homogeneous bond interfaces with no visible voids and microstructural features like splat boundaries, intersplat gaps, oxides, and porosities of metallic coatings [19,23]. For Al_2O_3-based ceramic coatings deposited using the OF technique, SEM observation showed no evidence of delamination. However, porosity formation occurred in the ceramic layers, and the coalescence of the pores led to cracking in the ceramic topcoats. Still, the size and intensity of these porosities depended on the TiO_2 content.

The porosity percentage of the ceramic layer was measured in five instances in various zones using image analysis. The average porosities of the A-0%T, A-3%T, A-13%T, and A-40%T ceramic finish layers fabricated by OF were 18.1%, 4.6%, 3.2%, and 1.64%, respectively. The Al_2O_3 coatings exhibited higher porosity, and an increase in TiO_2 content significantly reduced the coating porosity. The higher porosity of the Al_2O_3 coating finish layer could be attributed to the poor layering of insufficiently melted particles during the build-up of the thermally sprayed coating with the lower thermal energy of the OF technique (see Fig. 2a). Similarly, the lower porosity of the Al_2O_3-40% TiO_2 coating as compared with those of A, A-3%T, and A-13%T was due to the lower melting temperature, where its composition was close to that of the eutectic point (see Fig. 2b–d).

Fig. 3 shows cross-sectional SEM images at higher magnification of the microstructures of different nanostructured Al_2O_3-based finish layers with varying TiO_2 content (0, 3, 13, and 40%). The fabricated coatings showed a complex microstructure of partially melted particles, pores, inter-splat gaps, inherent pores, and vertical cracks. These microstructural features are common in ceramic coatings deposited via OF (thermal spraying) [8]. Unmelted and partially melted particles can remain inside the coating due to the powder injection trajectory, deposition in inhomogeneous turbulent flows, particle dispersion during thermal spraying, and particle size distribution of feed stock powder, which, for prospective researchers, is challenging to control. Resolidified or unmelted particles that are trapped in the coating microstructure are common sources of coating porosity, which severely affects the coating properties. Notably, the volume shrinkage of liquid droplets (or splats) caused by solidification and rapid cooling could generate pores, inter-splat gaps (grain edge), and vertical cracks inside the coating [24]. The nanostructure pure A-0%T finish layer shown in Fig. 3a contained only Al and O under different proportions and revealed an absence of contamination during OF deposition. In the case of the nanostructured A-3%T layer, as shown in Fig. 3b, the Ti content of zones D–F were 1.43, 19.39, and 1.53%, respectively. The figure shows that when the TiO_2 content increased, the colour changed from dark grey to white. In the case of the A-13%T finish layer with more homogenous distribution of Ti in the microstructure, as shown in Fig. 3c, the Ti content of regions G–I was 6.85, 6.86, and 6.63 wt%, respectively. In general, the lighter regions contained a higher concentration of Ti. In addition, the lamellar multilayer structure was produced by flame spraying in conjunction

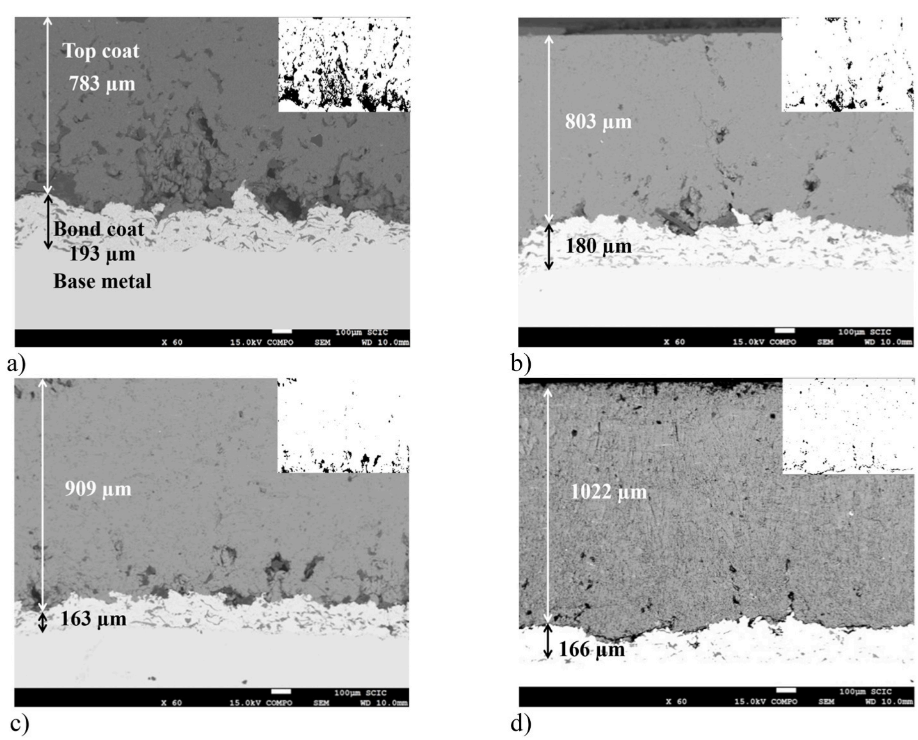

Fig. 2. SEM low magnification micrographs of cross section displaying the thickness of ceramic coatings and porosity evaluation: a) A-0%T, b) A-3%T, c) A-13%T, d) A-40%T.

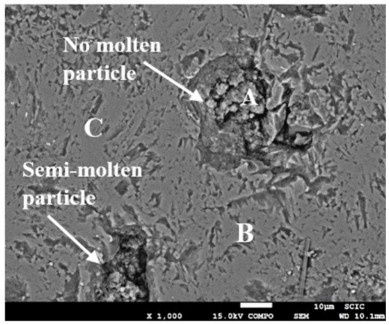

A-0%T			
Point	Al	O	Ti
A	48.57	51.43	(--)
B	46.06	53.94	(--)
C	54.68	45.32	(--)

a)

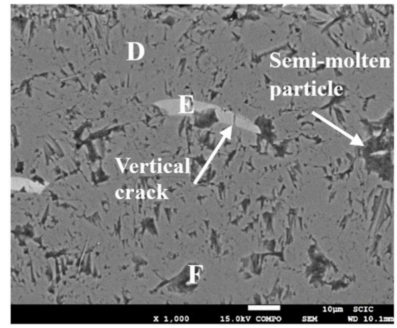

A-3%T			
Point	Al	O	Ti
D	46.76	51.81	1.43
E	30.77	49.84	19.39
F	42.43	56.04	1.53

b)

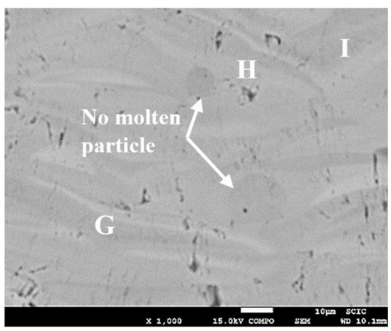

A-13%T			
Point	Al	O	Ti
G	39.93	53.23	6.85
H	41.18	51.78	6.86
I	7.04	52.57	6.63

c)

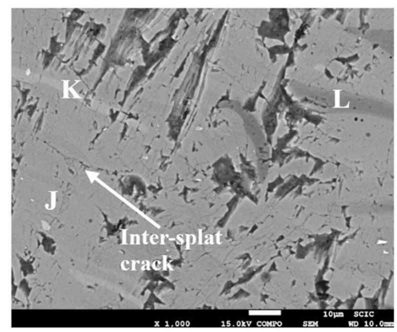

A-40%T			
Point	Al	O	Ti
J	30.07	49.89	20.05
K	22.00	48.56	29.44
L	29.63	48.57	21.80

d)

Fig. 3. High magnification cross-section SEM micrograph of nanostructured Al_2O_3-based with different TiO_2 content and EDX microanalysis.

with the impact, subsequent flattening, and successive stacking of splats, consistent with the findings in a previous study [25]. The stacking of melted particles enhanced diffusion at the grain boundaries and increased with TiO_2 concentration, thereby improving the homogeneity of Ti atom distribution in the A-13%T coating microstructure. In addition, the molten particles may form a single bath during the spraying process. This behavior occurs because the addition of TiO_2 lowers the melting point of the composite powders, enhancing the spreading effect of molten droplets. Consequently, this facilitates the movement of hot gases within the deposited ceramic layer, promotes a more uniform titanium distribution, and reduces porosity content [8,40]. In the case of the nanostructured A-40%T topcoat, as shown in Fig. 3d, the Ti contents of regions J–L were 20.05, 29.29, and 21.80 wt%, respectively. In addition, the nanostructured A-40%T coating exhibited a relatively higher number of vertical cracks due to the crystallographic anisotropy of the thermal expansion of the Al_2TiO_5 phase. Previous studies have reported the pseudobrookite structure of Al_2TiO_5 with an orthorhombic unit cell containing an Al^{3+} or Ti^{4+} cation surrounded by six oxygen ions, which forms a distorted oxygen octahedral. In our study, these structures induced crystallographic anisotropy, where the thermal expansion of the single crystal for crystallographic axes α_a, α_b, and α_c were $11.8 \times 10^{-6}/°C$, $19.4 \times 10^{-6}/°C$, and $-2.6 \times 10^{-6}/°C$, respectively [26]. In addition, the formation of the single crystal was promoted by the fine size of A-40%T particles and characterised by a larger surface area [27–29]. In the agglomerated powder, the total contact surface area between Al_2O_3 and TiO_2 was very high due to the small primary particles. In this case, Al_2O_3 and TiO_2 reacted as a unit and formed Al_2TiO_5. Due to the oxidation and decomposition into Al_2TiO_5, a significant reduction in the intermediate phase Al_2-xTi 1+ $x$$O_5$ was also observed [30]. As the small-sized Al_2O_3 and TiO_2 feedstock melted because of thermal spraying and resolidified during the cooling process, the microcracks formed and thermal stress was generated. These were inevitable with the drastic shrinkage difference in the various crystallographic axes, which caused the abrupt change in surface geometry [23]. The growth of Al_2TiO_5 by solid–solid reaction was due to the interdiffusion between Al_2O_3 and TiO_2 during cooling after the deposition process. These cracks appeared after the formation of Al_2TiO_5, which was brittle to the point that cracking occurred in the diffusion interface.

3.2. XRD analysis

XRD analytical results of the as-delivered feedstock powder and as-sprayed coatings are shown in Fig. 4. The phase of the OF coating was distinct from that of the as-delivered feedstock nanostructured powder. During deposition of the nanostructured feedstock, melting and rapid solidification visibly transformed the phases of the material. Phase composition of pure alumina (A-0%T) feedstock consisted of only stable α-Al_2O_3, whereas the. Coatings after deposition were primarily composed of γ-Al_2O_3 and the small remaining amounts of α-Al_2O_3 (see Fig. 4a). As reported in previous research, α-Al_2O_3 manifests as a stable Hexagonal Close-Packed (HCP) structure. However, γ-Al_2O_3 forms

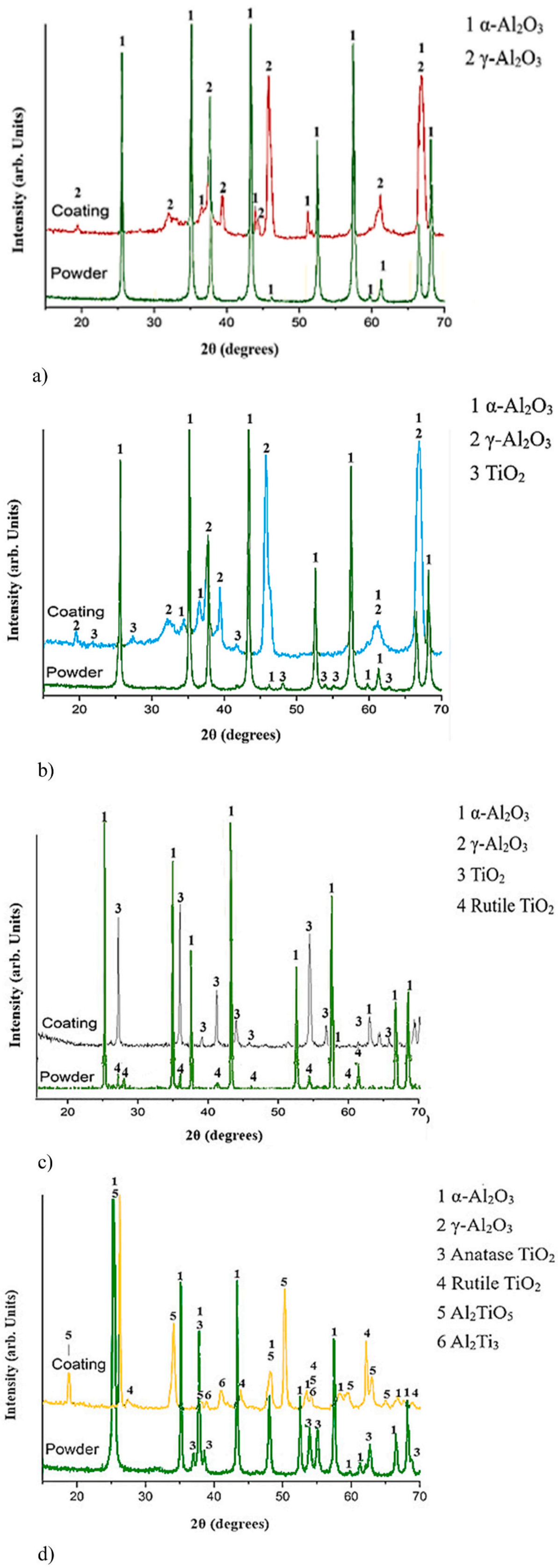

Fig. 4. XRD Patterns of Al_2O_3–TiO_2 spraying feedstocks powder and deposited coatings: a) A-0%T, b) A-3%T, c) A-13%T, d) A-40%T.

metastable cubic structures [17,31,32]. As the cooling rate of the Al_2O_3 splat was reasonably expeditious, it could not be transformed into α-Al_2O_3. Instead, metastable phases (γ) readily formed. The A-3%T and A-13%T coatings, as shown in Fig. 4b and c, respectively, presented typical spectra of α-Al_2O_3, γ-Al_2O_3, and TiO_2 as powder in the after-spraying process (as-sprayed), and no phase modification was observed. In addition, the A-40%T coating exhibited a different phase composition than that of the feedstock powder, Fig. 4d. Following the thermal spraying process, the dominating phase was metastable tialite Al_2TiO_5 with a pseudobrookite structure, which is clearly related to the Al_2O_3–TiO_2 phase diagram [33,34]. Tialite is formed from the reaction of Al_2O_3 and TiO_2 in hot OF plums. In this case, Al_2O_3 and TiO_2 react to form Al_2TiO_5, and the smaller alumina and TiO_2 particle sizes enhance the advanced reaction processes to form this phase [35]. In addition, the XRD pattern of this coating indicates the formation of Al_2Ti_3 with a trigonal bipyramid geometry (equatorial flatness) that includes three titanium atoms. Here, the atoms of aluminium are located at the vertices [36]. According to previous studies, TiO_2 exists in many polymorphs, of which rutile is the most thermodynamically stable. Bulk anatase TiO_2 is usually a metastable phase at room temperature (present in the initial powder of A-40%T). Accordingly, the phase transformation of bulk rutile TiO_2 to anatase TiO_2 occurs during the thermal spraying and cooling processes. However, the stability of TiO_2 polymorphs is dependent on the particle size and doping levels. Al_2O_3–TiO_2 has a high tendency to form different phases and undergo crystallographic structure changes depending on the material spray conditions, deposition technique, cooling process, proportion of each component, thermally sprayed parameters, and characteristics of the bounding layer [29].

3.3. Microhardness evaluation

Fig. 5a shows the microhardness of the Al_2O_3-based coatings under varying TiO_2 contents, and Fig. 5b shows a histogram of the average microhardness values and standard deviation of the ceramic topcoats. The Vickers microhardness along the cross section of the deposited coatings from the substrate base metal to the ceramic topcoat was measured for 10 instances. The average hardness values of A-0%T, A-3%T, A-13%T, and A-40% TiO_2 were 1317.9 ± 76.5, 1135.6 ± 51.4, 1021 ± 37.5, and 705 ± 96.4 $HV_{0.2}$, respectively. The comparable hardness values of A-%T, A-3%T, and A-13%T could be attributed to the identical same phase structure (α-Al_2O_3 matrix) of these coatings. The presence of unmelted particles in the coatings and the higher amount of α-Al_2O_3 than that of γ-Al_2O_3 helped to increase the microhardness [37,38]. Moreover, their hardness ranges were consistent with those reported in previous studies on Al_2O_3-based coatings [8,39]. The full melting of the powder is believed to help in the formulation of homogeneous distribution of Ti and O and to increase their toughness. The hardness of the A-40%T topcoat diminished significantly. This decrease in microhardness could be attributed to the formation of the Al_2TiO_5 phase (700 HV_{100}), which contained numerous microcracks and poor plate adhesion.

3.4. Friction coefficient and energy dissipation

The friction coefficient curves for the examined A-0%T, A-3, A-13, and 40% TiO_2 coatings under lubrication conditions were recorded during the friction tests at a normal load of 20 N and sliding speed of 0.07 m/s and are plotted as a function of time in Fig. 6. The friction coefficient was found to change with increasing TiO_2 content. Specifically, the initial friction coefficient increased rapidly but with unsteady oscillation, mainly because the movement of the friction pair was hindered by many microprotrusions on the contact area, leading to vibration and irregular noise. This caused an increase in the true contact area with a reduction in the initial surface roughness of the friction pairs. The variations in the curves then became approximately constant, and the friction coefficient values stabilised (to the steady state).

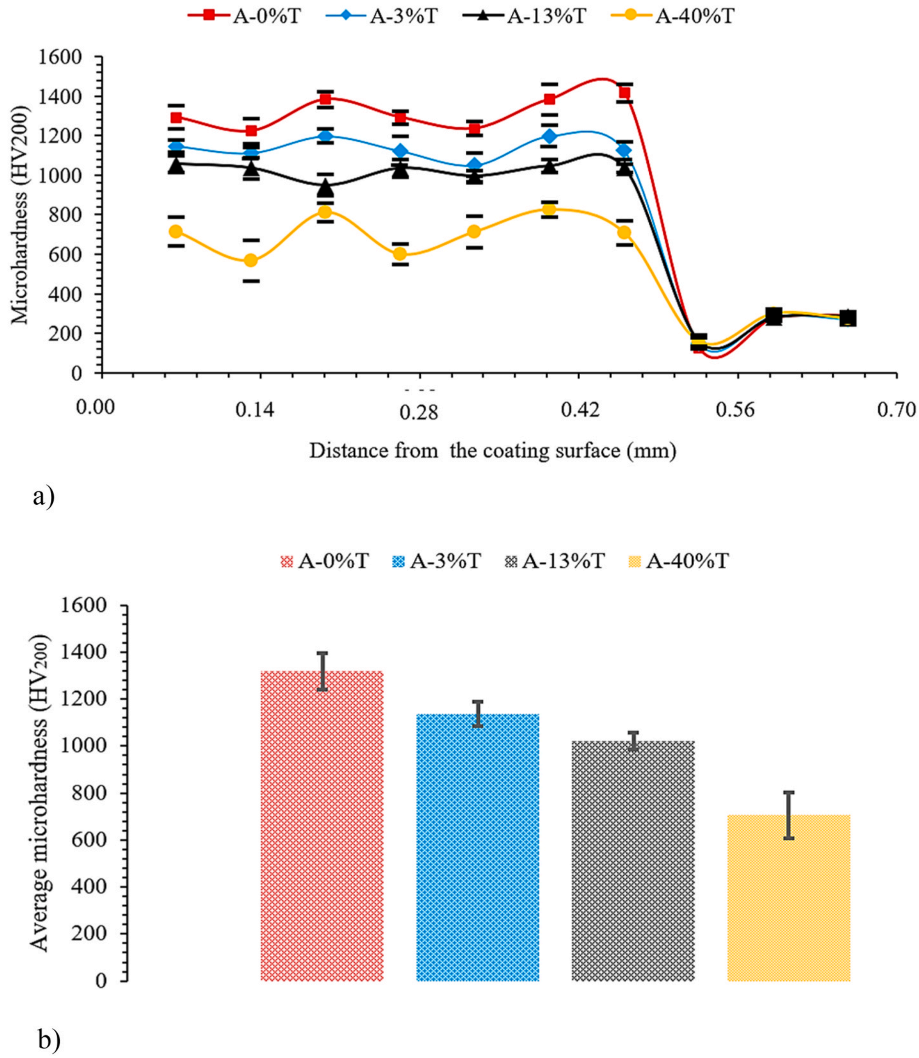

Fig. 5. a). Variation of microhardness in ceramics coating with different proportion of TiO_2 content and b) histogram of the average microhardness values and standard deviation of ceramic topcoats.

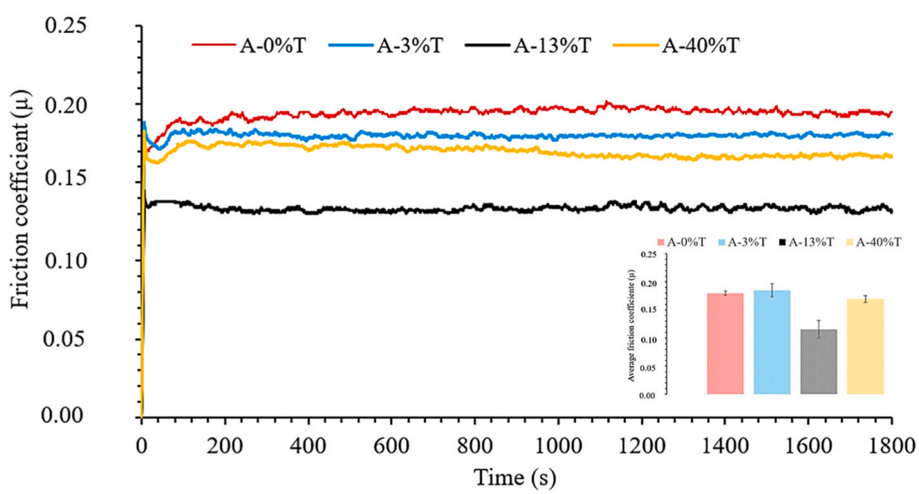

Fig. 6. Friction coefficient as a function of sliding time for nanostructures A-0%T, A.3%T, A-13%T and A-40%T, histogram of the average friction coefficient values and the standard deviations for different friction pairs.

The specimens behaved differently depending on the percentage of titania under the investigated conditions. In fact, the A-0%T, A-3%T, and A-40%T coatings recorded maximum friction coefficient values of approximately 0.184 ± 0.007, 0.171 ± 0.011, and 0.172 ± 0.004, respectively, whereas the coating reinforced with 13 wt% TiO_2 demonstrated a lower friction coefficient value of approximately 0.128 ± 0.007 as compared with other compositions (0, 3 and 40%).

The higher friction coefficients of the A-0%T and A-3%T coatings can be attributed to their higher hardness values (1317.9 HV and 1135.6 HV, respectively), with hardness ratios of HV_p/HV_{di} = 1.42 and 1.22, as compared to the disc's hardness (930 HV). Thus, high frictional resistance was expected. whereas the high friction coefficient of A-40%T with a lower hardness (705 HV) and hardness ratio of 0.76 could be linked to the high cracks and weak cohesion between splats due to the formation of the Al_2TiO_5 brittle phase. Fig. 7 shows that the excessive fracture and detachment of loosely bonded particles were dominant during the friction process (removal of the coating splats) and may have contributed to the enlargement of the real contact area, hindering the sliding movement of the mating pair. The reduced stability of the lubrication layer was probably due to a lower lubricant supply, which in turn increased the friction by the mechanism of third-body particles at the friction pair interface. Our results indicate that the A-13%T samples achieved a low coefficient of friction (~0.128), with a hardness of 1021 HV and a hardness ratio of 1.1. which was lower than those of the pure A-0%T, A-3%T, and A-40%T samples.

This low-friction behaviour could be related to the microstructure. Microstructural analysis as conducted in previous studies showed that the A-13%T coating with a hardness ratio of 1.1 has a relatively uniform (homogenous) distribution of TiO_2 in the Al_2O_3 matrix, a dense microstructure with splats that strongly bond to each other, and a higher coating toughness [8,40]. In our study, this may have helped to reduce the tangential or frictional forces, thus leading to a lower friction coefficient. In addition, the relatively high hardness and strong cohesion between the splats of this coating may have affected its deformability, resulting in a reduced ability of the counterpart disc material to adhere to the coating.

Table 3 shows that the energy dissipation (tribocontact friction loss) should exhibits an inversely proportional relationship with TiO_2 content for the A-0%T, A-3%T, and A-40%T coatings. According to Chen et al. [41], energy dissipation during the friction test can be evaluated as follows:

$$E = F_n \bullet v \int \mu \, dt \tag{1}$$

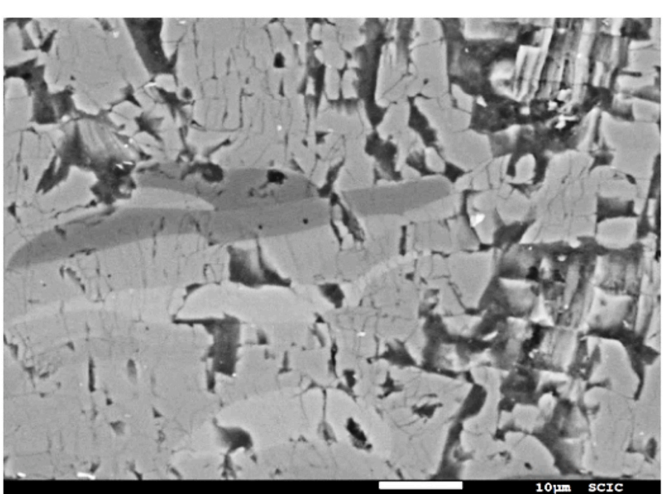

Fig. 7. The surface damage during friction process of A-40%T coating.

Table 3
Polynomial model constants and value of frictional energy losses.

Sample	a	b	c	Energy (J)
A	−0,0007	0,0226	0,0179	3035.42
A-3%T	−0,0009	0,0248	0,0178	2939.33
A-13%T	−0,0005	0,0153	0,0115	1972.32
A-40%T	−0,0007	0,0223	0,0118	2851.97

$$F_t = \mu \bullet F_n \tag{2}$$

$$F_t = \int \mu f \Big(F_n \tag{3}$$

$$E = \int \mu f(F_n) \, dF_n \bullet v \int dt \tag{4}$$

$$\mu f(F_n) = -aF_n^2 + bF_n + c \tag{5}$$

$$E = \left(-a\frac{F_n^3}{3} + b\frac{F_n^2}{2} + cF_n \right) \bullet v \bullet t \tag{6}$$

where F_n is the applied friction load (20 N), v is the linear velocity (0.07 m/s), and μ is the average kinetic friction coefficient during a travel time of 7200 s. The energy consumed by the A-0%T, A-3%T, A-13%T, and A-40%T coatings were 3035.42 J, 2939.33 J, 1972.32 J, and 2851.97 J, respectively. With the A-13%T coating, the energy consumed was reduced to approximately 1972.32 J.

The average values of the friction coefficient evolution as a function of the applied loads for Al_2O_3 under different percentage of TiO_2 are displayed in Fig. 8. The friction coefficients of all the ceramic coatings increased abruptly at the beginning of the sliding test. This may have been due to the topography of the initial surface roughness or the fresh surface, which influenced the contact intensity of the friction pairs. The variations in the curves then became relatively stable when the applied load exceeded 9 N. This occurred because when the applied load was increased, a higher number of asperities on the surface of the friction pair experienced contact and/or were embedded (depending on the hardness ratio). Therefore, the time required for the friction coefficient to achieve a stable state decreased, and the running-in period increased. However, a clear polynomial of degree 2 trend was observed in the relationship between the coefficient of friction and normal applied load. In the A-0%T, A-3%T, and A-40%T coatings, the average coefficient of friction depended on the load and differed for individual sliding couples only within a narrow range of values. The results confirmed that the coefficient of friction remained constant under an increasing load. Higher friction coefficient values for the A-0%T and A-3%T coatings were probably due to reduced lubricant supply, which was the result of the boundary layer film being adsorbed onto the contact surface to a certain degree. For the A-40%T sliding couple, the higher friction coefficient could be attributed to the large number of ceramic particles trapped in the contact area, which absorbed the lubricating oil and hindered the formation of a continuous lubrication layer between sliding contact surfaces. In addition, the friction and load action caused abrasive wear of the softer parts of friction paris. Notably, for all the contact loads, the friction coefficient of A-13%T was significantly reduced as compared with those of the other samples. This may have been due to the enhanced stability of the boundary-layer formation over the surfaces of the friction pair, which significantly affected the reduction in asperity contact. In addition, the pre-existing porosity and microcracks that were well distributed on the coating surface may improve the management of the friction coefficient of this type of coating in lubrication condition [42].

Fig. 9 illustrates the effects of the initial hardness ratio (HV_p/HV_d) on the friction coefficient under different applied loads and its obvious dependence on the type of coating (A-0%T, A-3%T, A-13%T, and A-40%

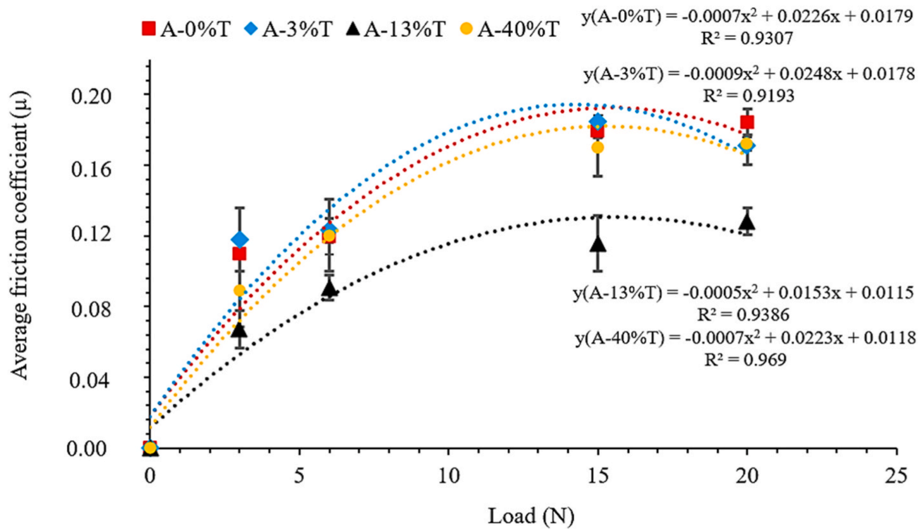

Fig. 8. Variation of coefficient of friction as a function of normal load for the different nanostructured coatings, A-0%T, A-3%T, A-13%T and A-40%T.

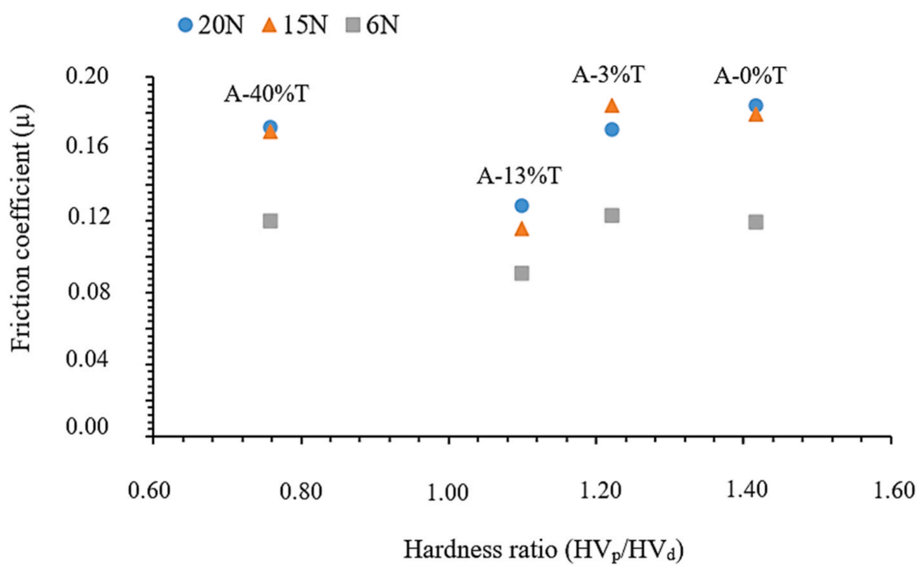

Fig. 9. Dependence of the friction coefficient on the hardness ratio under varying applied loads.

T) based on the different hardness ratios of 1.42, 1.22, 1.1, and 0.76, respectively. However, no correlation was observed between the coefficient of friction and the hardness ratio. As observed, when the applied load increased from 6 to 15 N, the friction coefficient increased from 0.120 ± 0.011 to 0.180 ± 0.2 (50%) for Al-0%T and to 0.123 ± 0.007 for A-3%T (49.98%), and from 0.120 ± 0.20 to 0.172 ± 0.004 for A-40% T (40.88%). In addition, with the increase in the applied load to 20 N, a slight variation was observed in the friction coefficient of 0.0917 ± 0.007 to 0.128 ± 0.007 (27.38%). No drastic changes were observed in the friction coefficient for the thermally sprayed A-13%T with an increase in the normal load. This enhancement could be attributed to the stability of the lubricant layer in its ability to withstand the load on moving surfaces (boundary layer), reduce friction between rubbing or sliding surfaces, and improve the load-carrying capacity of the thermally sprayed A-13%T coating under a hardness ratio of 1.1, thus revealing an exponential augmentation in its performance and stability at applied loads. Alternatively, boundary lubrication may be characterised as a regime in which the load is borne by the surface roughness rather than by the lubricant itself [43].

3.5. Stribeck curve study

3.5.1. Analysis of lubrication regimes

The Stribeck curve is used to analyse the friction behaviour as a function of oil viscosity (η), speed (v), and applied load (P_a) (Hersey number) [19,44,45]. To determine the effects of TiO_2 on the tribological properties of Al_2O_3-based materials, exploring the lubrication regimes of nanoscale Al_2O_3 and Al_2O_3 samples with different TiO_2 contents is crucial. The variations in the friction coefficient (μ) and lubrication regime as functions of different sliding speeds are plotted in Fig. 10. The figure shows that the lubrication regime changes as the sliding speed increases under a constant load. To clarify the effects of TiO_2 content on the transition between lubrication regimes, the average friction coefficient was determined by calculating the average value of all instantaneous friction coefficients when the friction was relatively stable.

For Al_2O_3-based coatings with different TiO_2 contents (0, 3, 13, and 40%), the coefficient of friction decreased from 0.21 to 0.186 for pure A-0%T, from 0.2 to 0.182 for A-3%T, and from 0.194 to 0.161 for A-40%T as the sliding speed increased from 0.03 to 0.21 m/s (see Fig. 10). This could be explained by the lubricant's ability to slightly reduce friction,

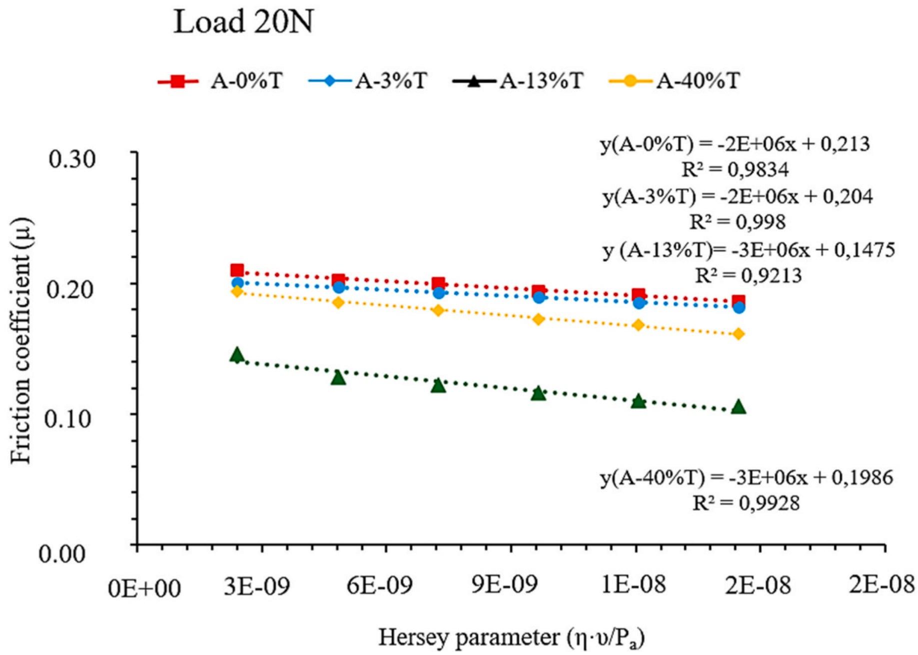

Fig. 10. The Stribeck curve at constant load and different sliding velocities for the friction pair F-5220 hardened steel and Al_2O_3-based coatings.

which slowed the flow of lubricant oil at microscopic levels. The A-13%T coating exhibited the lowest friction coefficient (0.146–0.106) over the same range of sliding speeds. This could be attributed to the coating microstructure and optimal hardness ratio between the ceramic pin and steel disc, which aid in generating a thin adsorbed lubricant film on the frictional surface, thereby reducing the friction coefficient during contact. In addition, the Hersey number remained constant for all deposited coatings, varying from 2.41×10^{-9} to 1.45×10^{-8}.

3.5.2. Hardness evolution

The evolution of the Vickers microhardness indentation of the hardened and tempered steel disc counterpart (F-5220) was investigated after 450 m of lubricated sliding distance, where the sliding speed (0.04, 0.07, 0.11, 0.14, 0.18 and 0.21 m/s) was increased by 0.036 m/s after each 75-m interval by means of work hardening (i.e., strain hardening). A minimum of eight microhardness measurements were conducted in different zones of the steel disc wear track for each friction pair, and the average values were considered in this study. The experimental data indicate that the area within the wear track of the counterpart disc experienced an increase in hardness compared with the unworn surface of the disc (initial hardness) following the running-in period, which was consistent with previous studies [46,47]. Strain hardening evidently occurred during the friction process for the counterpart steel disc with different ceramic coatings. The results are listed in Table 4. The hardness gain of the counterpart steel disc decreased with the TiO_2 content of the Al_2O_3-based pin coatings, where the contact friction pair of the A-0%T coating versus steel disc showed an approximately 18% hardness gain, with A-3%T at 11%, A-13%T at 3%, and A-40%T at approximately 7%. This suggests that the observed gains in hardness were more pronounced in the friction pair with the A-0%T coating, which exhibited a higher surface hardness against the steel disc as compared with the hardness measured with the A-3%T, A-13%T, and A-40%T coatings. The increase in microhardness in the wear tracks further supported the occurrence of extensive plastic deformation, and the higher microhardness values corresponded to higher hardness ratios.

3.5.3. Relationship between initial and final hardness ratios

A key feature of our study is the use of the final hardness ratio of each friction pair to evaluate the tribological behaviour of the system. The final hardness ratio serves as a more accurate indicator of friction and wear effects and the useable life of components in practical applications. Previous studies have incorporated an initial hardness ratio into the Hersey number [38]. To enhance our understanding of the tribological behaviour of different friction pairs, assessing the relationship between the strain hardening induced by plastic deformation after friction tests and its effects on the hardness ratio of the friction pair and the lubrication regime is critical. This knowledge enables us to estimate lubrication regimes under specific working conditions for a given type of lubricant and specific materials in contact.

To account for the effects of the initial and final hardness ratios (H_p/H_d) on the Stribeck curve parameters, we first determined the evolution of the final microhardness over the wear track surface of the counterpart metallic disc following sliding friction tests of each friction pair. These pairs included ceramic pin coatings with varying TiO_2 contents (0, 3, 13, and 40%) after a sliding distance of 450 m. The results indicate a linear relationship between the initial and final hardness ratios before and after the friction tests, as shown in Fig. 11. A good correlation between the two variables was observed.

Directly measuring the final hardness ratio in industrial applications or in the design of kinematic pairs is difficult. Therefore, establishing a mathematical relationship between the initial and final hardness ratios of friction pairs (under 20 N and at speeds of 0.04, 0.07, 0.11, 0.14, 0.18

Table 4
Parameters of Stribeck curve for each hardness ratio H_p/H_d after 450 m tests distance.

Sample	μ_{max}	K_{min}	μ_{min}	K_{max}	R_{af} (μm)	H_p/H_{df}	mg/s	Hardness Δ ceramic pin/disc
A-0%T	0,209542	$1{,}9E^{-09}$	0,186042	1,14E-08	3.5	1.27	$2.27.\ 10^{-3}$	388
A-3% T	0,200083	$2{,}2E^{-09}$	0,181792	1,32E-08	2.5	1.1	$2.57.\ 10^{-3}$	206
A-13% T	0,146292	$2{,}44E^{-09}$	0,106	1,46E-08	2.2	0.99	$2.02.\ 10^{-3}$	91
A-40% T	0,193583	$3{,}5E^{-09}$	0,161333	2,1E-08	2.35	0.69	$3.98.\ 10^{-3}$	−225

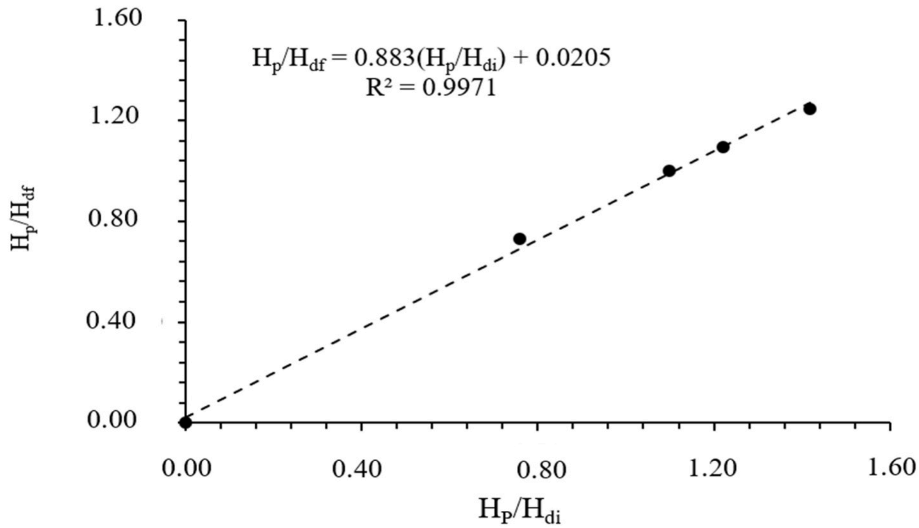

Fig. 11. Relationship between initial and final hardness ratio of friction pairs with different pairing materials; A, A-3%T, A-13%T and A-40%T ceramic coatings against hardened and tempered steel disc.

and 0.21) during the engineering material selection and design process would be useful. The relationship between the initial and final hardness ratios can be expressed as:

$$\frac{H_p}{H_{df}} = C_1 \bullet \frac{H_p}{H_{di}} + C_2 \tag{7}$$

In this linear relationship, C_1 simply amplifies or reduces the value obtained for HV_p/HV_{di} (initial hardness ratio), and C_2 is a constant. This work presents the equation derived from the experimental data as follows:

$$\frac{H_p}{H_{df}} = 0.883 \bullet \frac{H_p}{H_{di}} + 0.0205 \tag{8}$$

This study proposes incorporating the relationship between the initial and final hardness ratios into the Schipper's lubricant number, replacing the initial surface roughness. By integrating this fitted Equation (8) into the expression for the lubrication parameters (Hersey number, Z), we derived the following expression:

$$K = \frac{\eta \cdot v}{P_a \cdot 0.883 \cdot \frac{H_p}{H_{di}} + 0.0205} \tag{9}$$

A very strong correlation was observed between the final (H_p/H_{df}) and initial (H_p/H_{di}) hardness ratios. To further refine our analysis, we propose an alternative method for assessing the Stribeck curve parameters by examining the relationship between the hardness ratios of various ceramic coatings and the final hardness ratio (H_p/H_{df}).

As Fig. 12 shows, the correlation coefficients (R^2) indicate the valid dependence on the final hardness ratio. The generic model is linear and expressed as:

$$\mu . f\left(\frac{H_p}{H_{df}}\right) = m \cdot \left(\frac{\eta \cdot v}{P_a \cdot 0.883 \cdot \frac{H_p}{H_{di}} + 0.0205}\right) + \mu_0 \tag{10}$$

Moreover, the two terms that comprise the linear correlation model are the dependent term (m), which represents the slope, and the

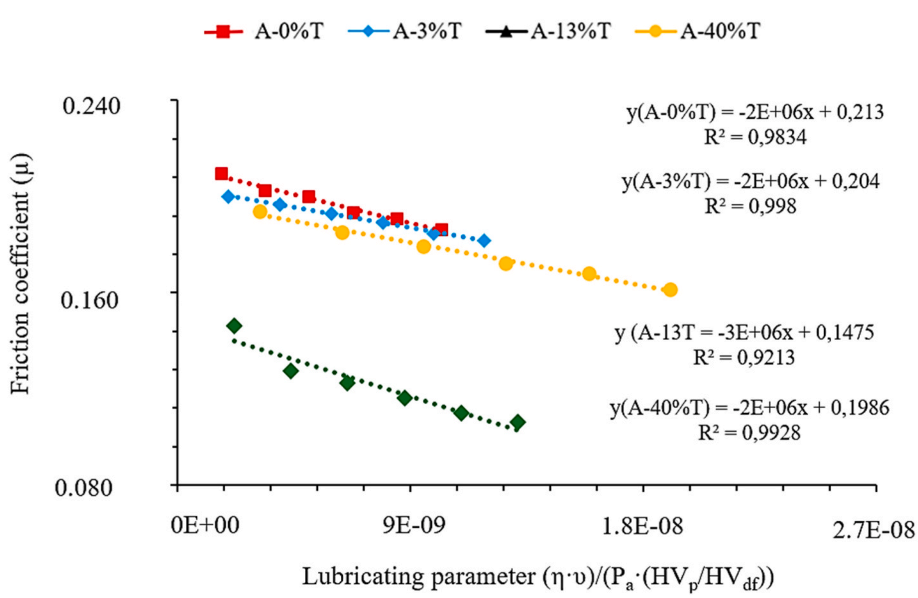

Fig. 12. The effect of new lubrication number (K) on friction coefficient for the A, A-3%T, A-13%T and A-40%T coatings sliding against hardened and tempered F-5220 steel disc friction pairs with different hardness ratio.

independent term (μ_o), which signifies the maximum friction coefficient (boundary lubrication) when the lubrication number K equals 0, thereby intercepting the y axis. This linear relationship clearly illustrates a qualitative increase in the coefficient of friction as a function of the final hardness ratio. By contrast, the friction pair consisting of A-13%T ceramic coating and F-5220 disc shows a steeper decline toward the x axis because of its high slope (m) of 3, resulting in a friction increase of approximately 33% as compared with the other friction pairs of A-0%T, A-3%T, and A-40%T.

The Stribeck curve represents the effects of incorporating the final hardness ratio (after a distance of 450 m) in the Hersey number for ceramic coatings. Fig. 12 shows the Stribeck curves for the ceramic coatings with different TiO_2 contents and contacts with hardened and tempered discs when utilising the new lubrication number.

The Stribeck-like curves all exhibited a linear plot tendency. Consequently, mixed lubrication regimes can be easily distinguished for each ceramic friction pair coating but with different slopes and lubrication numbers (see Table 4). Notably, an increase in the negative slope of the linear regression equation from (−2 E+6) for the A-0%T, A-3%T, and A-40%T coatings to (−3 E+6) significantly enhanced the lubrication conditions of the A-13% TiO_2 coating, resulting in reduced wear losses (mg/s). Therefore, to better control friction and wear, this criterion enables the prediction of the lubrication conditions of each friction pair, which depend on both the TiO_2 content and hardness ratio.

3.5.4. Wear behaviour

The results of the sliding wear tests on the sprayed coatings are summarised in Table 4. After each test, the wear rate (mg/s) was determined for different ceramic specimens. Mass losses were measured under an applied load of 20 N at different sliding speeds for the A-0%T, A-3%T, A-13%T, and A-40%Ti coatings. The results showed that the lowest wear occurred at an optimal hardness ratio (HV_{pin}/HV_{disc}) of approximately 1.1 under the different test conditions. The A-40%T samples, which had lower initial (0.76) and final (0.69) hardness ratios, demonstrated higher material loss, as reflected by their higher wear rates (mg/s). The higher material loss in these samples could be attributed to their fine microstructure, reduced splat adherence, and inter-splat crack patterns that developed from successive domain division due to sequential cracking during splat cooling [18,48,49]. These cracks tended to propagate through the splats, easily reaching the boundary between the ceramic coating and bond layer, thereby exacerbating material damage by complete spalling. The results underscore the significance of hardness ratio in evaluating a material's wear resistance. The identified wear mechanisms include abrasive wear, the formation of debris particles in the contact area, load, abrasive particle size, the mechanical properties of ceramic coatings, and as-sprayed defects. In addition, when correlating the wear results with the XRD phase analysis conducted in Ref. [50], we found that coatings rich in the α-Al_2O_3 phase, such as (like) A-0%T, A-3%T, and A-13%T, exhibited lower wear. Among these, the A-13%T coatings displayed the best overall tribological performance, characterised by a denser structure, an optimal hardness ratio (1.1), and better performance.

To better understand the differences in the tribological behaviour of the nanostructured coatings (A-0%T, A-3%T, A-13%T, and A-40%T), we examined the evolution of surface roughness on the wear track surfaces of the counterpart metallic disc after 450 m (see Table 4). Fig. 13 shows the highest surface roughness value of the counterpart metallic disc, recorded at 3.5 ± 0.11 μm, occurred under lubrication conditions against the A-0%T ceramic coating. By contrast, the surface roughness values of the A-3%T and A-40%T coatings were 2.5 ± 0.1 and 2.35 ± 0.04 μm, respectively. The lowest surface roughness of the metallic disc, at 2.2 ± 0.06 μm, was observed after it was rubbed against the A-13%T coating. The final surface roughness of the metallic disc increased by 93.6% after it was rubbed against the pure alumina coating (A-0%T). For the A-3%T and A-40%T coatings, the increases were 40.6% and 30.7%, respectively, whereas for the A-13%T coating, the increase was 21.1%. The variations in hardness ratios significantly affected the final topography and surface profile roughness (R_a) of the metallic disc. As the figure shows, the relationship between the wear track roughness of the metallic disc and the final hardness ratio was not linear. The results indicated that the A-3%T and A-40%T coatings exhibited higher wear than that of the A-0%T coating under the same experimental conditions. The wear behaviour of these ceramic coatings was influenced by the hardness ratio, microstructure, and defects including porosity, micro-cracks, and inter-splat boundaries. Notably, the A-13%T coating demonstrated significant differences in wear and coefficient of friction, benefiting from an optimal final hardness ratio of 0.99. This optimal ratio effectively inhibited crack initiation and propagation under stress during the friction and wear processes, resulting in an optimal increase in friction and wear for this coating.

Optical microscopy images of the wear track on the hardened and tempered F-5220 disc, after rubbing against the A-0%T pin, indicated an increase in surface roughness and wear rate (5.79E-03 ± 1.00E-03 mm^3/N.m). This was evidenced by a extensive number of wear scars and

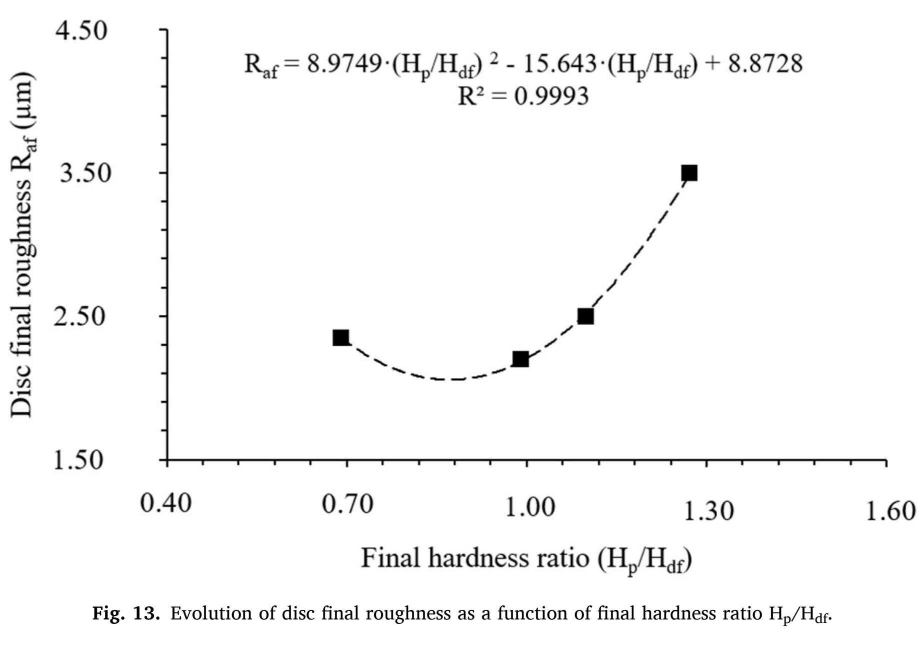

Fig. 13. Evolution of disc final roughness as a function of final hardness ratio H_p/H_{df}.

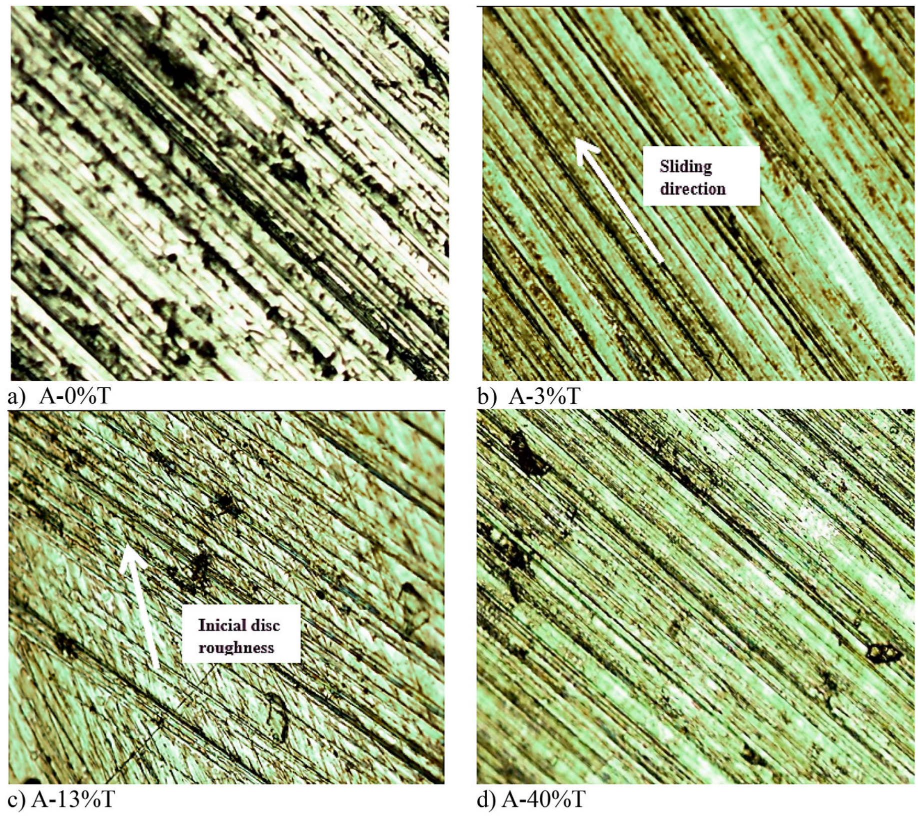

Fig. 14. Optical images of surface topography of steel counterpart disc in contact with ceramic coating pins; A-0%T, A-3%T, A-13%T and A-40%T (200X).

microgrooves and by plastic flow of the steel disc in a direction perpendicular to the sliding motion, as shown in Fig. 14a. The microgrooves were aligned parallel to the sliding direction. Plastic shearing of asperities was observed as extruded fins at the edges of the grooves formed during the rubbing process. These fins can detach to form secondary chips when cracks coalesce. In addition, the worn surface revealed step-sided grooves that corresponded in size to the abrasive particles and hard asperities that closely resembled cutting by a series of contact asperities. For the friction pairs contacting asperities A-3%T and A-40%T against a hardened and tempered disc, as shown in Fig. 14b and d, respectively, the wear rate (3.1 E−03 ± 9.9 E−04 and 2.11E-03 ± 3.9 E−04 mm^3/Nm, respectively) and the wear surface of the disc showed less damage and reduced plastic flow as compared with pure Al_2O_3 under identical sliding conditions. The friction pair containing A-13%T against the steel disc revealed that the wear rate (1.29 E−03 ± 5.77 E−04 mm^3/Nm) and the wear surface damage on the steel disc was relatively smoother, with less plastic flow and thus lower surface roughness, as shown in Fig. 14c. However, the relatively large variation in the experimental values of the surface roughness was attributed to a proportional increase in surface roughness with abrasive particle size until reaching the critical particle size. It was also determined by factors such as microstructure, lubrication condition, and the hardness ratio of each friction pair. Initially, we believed that abrasive wear was caused by grit and/or hard asperities that closely resembled cutting by a series of contacting asperities under lubrication conditions. In addition, the reduction in the debris size resulted in a lower surface roughness of the

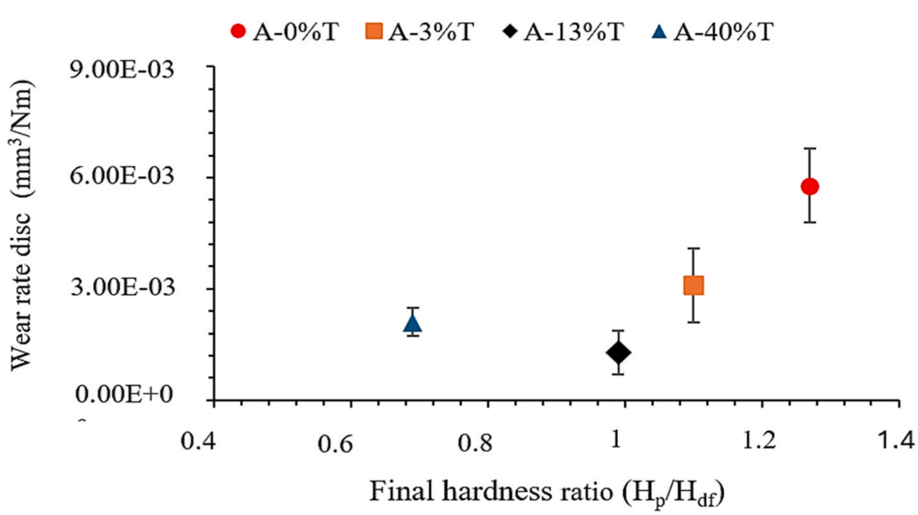

Fig. 15. Wear rate vs. final hardness ratio for the counterpart hardened and tempered steel F-5220 in lubrication conditions.

counterpart disc. The higher scratching (surface roughness) observed in the friction pairs with a higher hardness ratio of the nanostructured A-0%T and A-3%T coatings against the steel disc could be attributed to limited movement of debris particles derived from the higher protrusion of abrasives into the surface. This led to deeper penetration and a higher contact area that removed material from the steel disc surface via ploughing and microcutting [51,52]. A previous study demonstrated that the effects of debris on the tribological behaviour depend on variations in the size and distribution of wear debris [53]. Fig. 15 showed the evolution of disc wear rate influenced by the final hardness ratio. A optimal final hardness ratio (0.99) results in a lower friction coefficient and contributes to an decreased wear rate in lubricated conditions.

3.5.5. Evolution of the surface roughness of the counterpart steel disc

The surface roughness of the counterpart steel disc was analysed both inside and outside the wear track. The initial surface roughness was measured as 1.79 ± 0.081. Table 5 illustrates how the surface roughness changed after sliding 450 m against the four ceramic coatings (A-0%T, A-3%T, A-13%T, and A-40%T). In general, an increasing trend in surface roughness of the counterpart steel disc was observed, correlating with the hardness ratio between the four ceramic coatings and the steel disc (with a negative ratio indicating that the steel disc was harder). For the A-0%T and A-3%T coatings, significant changes in surface roughness of approximately 93% and 40%, respectively, were observed for positive hardness differences of 388 and 206, and final hardness ratios of 1.27 and 1.1, respectively. In these cases, the roughness of the counterpart disc increased to 3.5 ± 0.11 and 2.5 ± 0.1, respectively. By contrast, the lowest roughness value (21%) was observed with the A-13%T coating, which had a positive hardness difference of 91 and a final hardness ratio of 0.99. Here, the surface roughness of the counterpart disc increased to 2.2 ± 0.06 during the friction test. Although the hardness difference between the ceramic coating and counterpart disc was negative for the A-40%T sample, a significant change (approximately 30.7%) was detected, with a negative hardness difference of approximately −225 and a final hardness ratio of approximately 0.69, where the disc surface roughness increased to 2.35 ± 0.04. No clear trends or effects were observed on the surface roughness of the disc when various ceramic coatings were used for the pins. This lack of consistent results may relate to the A-40%T topcoat, which has a microstructure that is likely influenced by a brittle Al_2TiO_5 compound phase formed during thermal spraying and cooling. This phase affects crack development and, in turn, the mechanical properties of the coating. In addition, work hardening occurs due to plastic deformation, and evidence of work hardening can be observed by the increase in disc wear track hardness [54].

Table 5 summarises the results obtained from the friction tests and highlights the effects of the hardness ratio on the roughness and strain hardening of the steel disc investigated in this study.

Table 5
Surface hardness and surface roughness of the hardened and tempered F-5220 steel disc used in this study, measured before and after the tribology tests.

Sample	Disc final R_a (μm)	Δ R_a (%)	Initial hardness ratio	Final hardness ratio	Δ disc hardening (%)
A-0%T	3.5 ± 0.11	93.6	1.42	1.27	18
A-3%T	2.5 ± 0.1	40.5	1.22	1.1	11
A-13%T	2.2 ± 0.06	21	1.1	0.99	3
A-40%T	2.35 ± 0.04	30.7	0.76	0.69	7

4. Conclusion

The following conclusions were drawn from this study.

- The deposited coatings exhibited typical OF-sprayed characteristics, including cracks, pores, and voids, with TiO_2 content affecting powder melting. Higher TiO_2 improved porosity but decreased microhardness and negatively impacted mechanical and tribological properties. The A-13%T coating, with its uniform Ti distribution and low porosity, showed excellent friction and wear performance under lubrication, while the A-40%T coating, despite its low porosity, suffered from microcracking, grooving, and particle detachment during testing.
- The surface roughness of the ceramic samples reflected the effects of (OF) spraying, with R_a values of the steel disc counterpart increasing by 1.96, 1.4, 1.23, and 1.3 times when tested against A-0%T, A-3%T, A-13%T, and A-40%T coatings, respectively. Wear marks were deepest for A-0%T, A-3%T, and A-40%T coatings, while A-13%T produced shallower marks due to reduced abrasive wear. Detached fragments from the coatings acted as abrasive particles, impacting the steel disc surface. The wear track hardness significantly influenced lubrication conditions and Hersey numbers in the friction pairs.
- No significant differences in friction coefficients were observed for the A-0%T, A-3%T, and A-40%T coatings, indicating that neither chemical composition nor porosity substantially influenced the friction mechanism. The A-13%T coating demonstrated the best tribological performance due to its optimal hardness and α-Al_2O_3 matrix reinforced with γ-Al_2O_3 particles.
- The tribological properties of the coatings correlated with the hardness ratios of the friction pairs. The A-40%T coating suffered progressive damage and lubrication failure due to wear debris. A-0%T and A-3%T coatings, with hardness ratios of 1.27 and 1.22, showed higher friction coefficients and wear losses, leading to poor lubrication. In contrast, the A-13%T coating, with an optimal final hardness ratio of 0.99, achieved superior lubrication conditions and wear resistance, enabling the prediction of the K value for the onset of hydrodynamic lubrication based on pressure, sliding speed, and coating microstructure.
- A systematic approach to material selection is essential for identifying the most suitable materials for engineering applications. Our experiments classified the coatings into three categories based on their tribological performance: A-0%T and A-3%T exhibited the highest hardness, hardness ratios, friction coefficients, and wear; A-40%T showed the lowest hardness, hardness ratio, and the highest friction coefficient along with significant wear; while A-13%T demonstrated optimal initial and final hardness ratios (1.1 and 0.99), minimal friction, and reduced wear. This approach provides a novel framework for selecting friction pairs and coatings, improving performance and extending the lifespan of industrial components.

Declaration of competing interest

The authors declare that they have no known competing financial interests or personal relationships that could have appeared to influence the work reported in this paper.

Acknowledgments

David Leal Cano acknowledges the financial support of the Margarita Salas postdoctoral contract MGS/2021/10 (UP2021-021) financed by the European Union-Next Generation EU.

References

[1] Deng Y, Shichang D, Shiyao J, Chen Z, Zhiyuan X. Prognostic study of ball screws by ensemble data-driven particle filters. J Manuf Syst 2020;56:359–72.
[2] Munoz-Escalona P, Maropoulos PG. A geometrical model for surface roughness prediction when face milling Al 7075–T7351 with square insert tools. J Manuf Syst 2015;36:216–23.

[3] Wojciechowski S, Wiackiewicz M, Krolczyk GM. Study on metrological relations between instant tool displacements and surface roughness during precise ball end milling. Measurement 2018;129:686–94.
[4] Guo H, Li B, Yan P, Wu Z, Li F, Liu Z. Microstructures, mechanical properties and tribological behaviors of NiAl-based composite coatings with various addition of Nb. Surf Coating Technol 2022;449:128977.
[5] Guo H, Li B, Yan P, Wu Z. Microstructures, mechanical properties and tribological behaviors of HVOF-sprayed CoMoCrSi alloy coatings before and after 800° C-annealed treatment. J Alloys Compd 2022;909:164662.
[6] Guo H, Li B, Lu C, Zhou Q, Jia J. Effect of WC–Co content on the microstructure and properties of NiCrBSi composite coatings fabricated by supersonic plasma spraying. J Alloys Compd 2019;789:966–75.
[7] Lubrication mechanisms of Nb-contained oxides characterizing tribochemistry of NiAl/Nb/Ag composites coatings revealed by the density functional theory (DFT) computation. Tribol Int 2023;(182):108352.
[8] Habib KA, Saura JJ, Ferrer C, Damra MS, Giménez E, Cabedo L. Comparison of flame sprayed Al_2O_3/TiO_2coatings: their microstructure, mechanical properties and tribology behavior. Surf Coating Technol 2006;201(3–4):1436–43.
[9] Zhang L, Liao XJ, Zhang SL, Luo XT, Li CJ. Effect of powder particle size and spray parameters on the Ni/Al reaction during plasma spraying of Ni-Al composite powders. J Therm Spray Technol 2021;30:181–95.
[10] Rastegar F, Richardson DE. Alternative to chrome: HVOF cermet coatings for high horsepower diesel engines. Surf Coat Technol 1997:156–93.
[11] Champagne VK, Helfritch DJ. Mainstreaming cold spray-push for applications. Surf Eng 2014;30:396–403.
[12] Jones R, Matthews N, Rodopoulos CA. On the use of supersonic particle deposition to restore the structural integrity of damaged aircraft structures. Int J Fatig 2011; 33:1257–67.
[13] Klyatskina E, Espinosa-Fernández L, Darut G, Segovia F, Salvador MD, Montavon G, Agorges H. Sliding wear behavior of Al_2O_3 -TiO_2coatings fabricated by the suspension plasma spraying technique. Tribol Lett 2015;59:1–9.
[14] Birleanu C, Pustan M, Cioaza M, Molea A, Popa F, Contiu G. Effect of TiO_2 nanoparticles on the tribological properties of lubricating oil: an experimental investigation. Sci Rep 2022;12(1):5201.
[15] Restrepo E, Monsalve M, Gonzalez A, Vargas F, Latorre G, López E. Influencia de los esfuerzos residuales en la adherencia de recubrimientos de Al_2O_3-40% TiO_2 depositados mediante proyección térmica por combustión. Bol Soc Espanola Ceram Vidr 2016;55(6):219–27.
[16] Klyatskina E, Rayón E, Darut G, Salvador MD, Sánchez E, Montavon G. A study of the influence of TiO_2 addition in Al_2O_3 coatings sprayed by suspension plasma spray. Surf Coating Technol 2015;278:25–9.
[17] Eraslan FS, Gecu R. Enhancing wear and corrosion resistance of TiO_2–Al_2O_3 hybrid coatings by the development of TiO_2–Al_2O_3 bilayer film coatings. Ceram Int 2014.
[18] Eraslan FS, Gecu R. Chemical composition optimization of Al_2O_3-TiO_2 composite coatings for enhanced wear and corrosion resistance. Surf Coating Technol 2023; 474:130053.
[19] Eraslan FS, Turu IC, Ozcan M, Birol B, Gecu R. Influence of layer number and sintering temperature on microstructural, tribological, and corrosion behavior of Al_2O_3-TiO_2 multilayer coatings. Ceram Int 2023;49(20):33226–35.
[20] Guo H, Yan P, Wu Z, Li B, Li F, Hu J, Chen Z. Lubrication mechanisms of Nb-contained oxides characterizing tribochemistry of NiAl/Nb/Ag composites coatings revealed by the density functional theory (DFT) computation. Tribol Int 2013;182: 108352.
[21] Guo H, Li B, Yan P, Wu Z, Li F, Wang Z, Liu Z. Microstructure and tribo-mechanical properties of APS-sprayed NiAl/Cr_2AlC composite coatings with various additions of self-made Cr_2AlC. Surf Coating Technol 2013;457:129302.
[22] Shaw LL, Goberman D, Ren R, et al. The dependency of microstructure and properties of nanostructured coatings on plasma spray conditions. Surf Coat Technol 2000;130(1):1–8.
[23] Kwon H, Yoo YW, Park Y, Nam UH, Byon E. Effect of TiO2 on mechanical and thermal properties of Al_2O_3-based coating via atmospheric plasma spraying. Journal of Asian Ceramic Societies 2023;11(2):282–90.
[24] Habib KA, Cano DL, Serrano Mira J, Encinas Emilio Rayón, Dosta RS. Impact of microstructure on remelting parameters and mechanical behavior of thermally sprayed NiCrBSi coating. J Therm Spray Technol 2024;33(1):290–307.
[25] Parco M, Zhao L, Zwick J, Bobzin K, Lugscheider E. Investigation of particle flattening behaviour and bonding mechanisms of APS sprayed coatings on magnesium alloys. Surf Coating Technol 2007;201(14):6290–6.
[26] Papitha R, Suresh MB, Das D, Johnson R. Effect of micro-cracking on the thermal conductivity and thermal expansion of tialite (Al_2TiO_5) ceramics. Process Appl Ceramic 2013;7(3):143–6.
[27] Hassan AM, Naga S, Awaad M, Saleh A. Formation, phase stability, and characterization of unstabilized aluminum titanate (Al_2TiO_5). Ceramics 2021.
[28] Zheng J, Hu X, Ren Z, Xue X, Chou K. Solid-state reaction studies in Al_2O_3–TiO_2 system by diffusion couple method. ISIJ Int 2017;57(10):1762–6.
[29] Vargas F, Ageorges H, Fournier P, Fauchais P, López ME. Mechanical and tribological performance of Al_2O_3-TiO_2 coatings elaborated by flame and plasma spraying. Surf Coating Technol 2010;205(4):1132–6.
[30] Buscaglia V, Nanni P. Decomposition of Al_2TiO_5 and Al_2 (1-x) MgxTi (1+ x) O_5 ceramics. J Am Ceram Soc 1998;81(10):2645–53.
[31] Di Girolamo G, Brentari A, Blasi C, Serra E. Microstructure and mechanical properties of plasma sprayed alumina-based coatings. Ceram Int 2014;40(8): 12861–7.
[32] Kim HS, Park NK, Lee TJ, Kang M. Effect of AlF_3 seed concentrations and calcination temperatures on the crystal growth of hexagonally shaped α-alumina powders. Ceram Int 2014;40(2):3813–8.
[33] Feng CF, Froyen L. Formation of Al_3Ti and Al_2O_3 from an Al–TiO_2 system for preparing in-situ aluminium matrix composites. Compos Appl Sci Manuf 2000;31 (4):385–90.
[34] Tsetsekou A. A comparison study of tialite ceramics doped with various oxide materials and tialite–mullite composites: microstructural, thermal and mechanical properties. J Eur Ceram Soc 2005;25(4):335–48.
[35] Kim D, Kim HJ, Kim HT, Namkung J, Kim I, Choi SC, Ryu SS. Mechanical properties of Al_2TiO_5 ceramics for high temperature application. Curr Nanosci 2014;10(1):54–158.
[36] Richter A, Berger L-M, Conze S, Sohn YJ, Vassen R. Emergence and impact of Al_2TiO_5 in Al_2O_3-TiO_2 APS coatings. Mater Sci Eng 2019;480:012007 [CrossRef].
[37] Michalak M, Łatka L, Sokołowski P, Candidato RT, Ambroziak A. Effect of TiO_2 on the microstructure and phase composition of Al_2O_3 and Al_2O_3–TiO_2 APS sprayed coatings. Bull Pol Acad Sci Tech Sci 2021;69(2).
[38] Michalak M, Łatka L, Sokołowski P. The microstructure and selected mechanical properties of Al_2O_3 + 3 wt.% TiO_2 plasma sprayed coatings. Weld Technol Rev 2019;91(6):39–45.
[39] Habib KA, Leal Cano D, Serrano Mira J, Rayón E, Abellán-Nebot JV, Dosta S. Tribology behaviour of graphene-modified nanostructured Al_2O_3/3% TiO_2 coatings under boundary and mixed lubrication conditions. Wear 2024;548–549: 205381.
[40] Ghazali MJ, Forghani SM, Hassanuddin N, Muchtar A, Daud AR. Comparative wear study of plasma sprayed TiO_2 and Al_2O_3–TiO_2 on mild steels. Tribol Int 2016;93: 681–6.
[41] Chen X, Qin X, Zhu Z, Gao K. Microstructural evolution and wear properties of the continual local induction cladding NiCrBSi coatings. J Mater Process Technol 2018; 262:257–68.
[42] Hardwick C, Lewis R, Stock R. The effects of friction management materials on rail with preexisting rcf surface damage. Wear 2017;384:50–60.
[43] Boiko MV, Sidashov AV, Boiko TG, Burykin IV, Uflyand IE. The mechanism of formation of boundary lubricating films during friction in a medium of di (2-ethylhexyl) sebacate. Tribol Int 2022;165.
[44] Woydt M, Wäsche R. The history of the Stribeck curve and ball bearing steels: the role of Adolf Martens. Wear 2010;268(11–12):1542–6.
[45] Ali MKA, Xianjun H, Mai L, Qingping C, Turkson RF, Bicheng C. Improving the tribological characteristics of piston ring assembly in automotive engines using Al_2O_3 and TiO_2 nanomaterials as nano-lubricant additives. Tribol Int 2016;103: 540–54.
[46] Clarke A, Weeks IJJ, Snidle RW, Evans HP. Running-in and micropitting behaviour of steel surfaces under mixed lubrication conditions. Tribol Int 2016;101:59–68.
[47] Vrček A, Hultqvist T, Johannesson T, Marklund P, Larsson R. Micro-pitting and wear characterization for different rolling bearing steels: effect of hardness and heat treatments Wear, vol. 458; 2020, 203404.
[48] Moshkovich A, Perfilyev V, Gorni D, Lapsker I, Rapoport L. The effect of Cu grain size on transition from EHL to BL regime (Stribeck curve). Wear 2011;271(9–10): 1726–32.
[49] Chen L, Yang GJ, Li CX, Li CJ. Hierarchical formation of intrasplat cracks in thermal spray ceramic coatings. J Therm Spray Technol 2016;25:959–70.
[50] Bolzoni L, Yang F. X-ray diffraction for phase identification in Ti-based alloys: benefits and limitations. Phys Scripta 2024;99(6):065024.
[51] Feng X, Kwon S, Park JY, Salmeron M. Superlubric sliding of graphene nanoflakes on graphene. ACS Nano 2013;7(2):1718–24.
[52] Guo Y, Guo W, Chen C. Modifying atomic-scale friction between two graphene sheets: a molecular-force-field study. Phys Rev 2007;B 76(15):155429.
[53] Li W, Zhang LC, Wu CH, Cui ZX, Niu C, Wang Y. Debris effect on the surface wear and damage evolution of counterpart materials subjected to contact sliding. Advan Manufact 2022:1–15.
[54] Maier M, Pusterhofer M, Summer F, Grün F. Validation of statistic and deterministic asperity contact models using experimental Stribeck data. Tribol Int 2022;165:107329.

Dr, Dr. Kudama Habib Ameen

Industrial Engineer from Baghdad University in 1981–1982 PhD in Industrial Engineering from the Polytechnic University of Valencia in 1993, with a thesis entitled "Investigation on the stability of Lubricants layers in the metal-ceramic friction under simulated conditions of piston compression rings and cylinder liner of internal combustion engines".

He started his career in the industry chaining responsibilities in different activities such as heat and surface treatment, welding and joining, machining processes until 1984. In 1985 was named as DG of the establishment. In 1988 was enjoy an exchange scholarship for follows his doctoral thesis at the Polytechnic University of Valencia. Finished his doctoral studies in 1993 and rejoined the Ministry of Industry as Head of R & D center and also as a part-time professor at the University of Baghdad.

In 1995 he joined as a full professor in the Altahady/Libyan University in the Dpt.of. Mechanical Engineering and Design until 1997 when he rejoined as a postdoctoral researcher in the Department of Mechanical and Materials Engineering of the UPV. In 1998 start his job at the UJI in the Area of Materials Science and Metallurgical Engineering, as full time Associate Professor and from 2004 to the present, deals as senior lecturer, teaching decency in the degrees of Mechanics Engineering specialty, Industrial Engineering and degrees in mechanical engineering, Industrial Technology and Electrical Engineering. Also he teaches in the Masters in Science, Technology and Applications of Ceramic Materials and Design and Manufacture. He has been tutor and coordinator of the ERASMUS of Mechanical Engineering and Industrial Engineering.

Actually, he is the A member of the Manufacturing Process Engineering Department Engineering, having led projects and agreements with companies in the lines of metals thermal spraying, high temperature corrosion, tribology (friction, wear and lubrication) , welding and joining and fracture mechanics. He has directed several doctoral theses and he is author of several international indexed publications related to their research topics, and more than 25 communications in national and international conferences

David Leal Cano

Dr. David Leal Cano Doctor in Materials and Industrial Technologies, extensive professional experience in the field of tribology (friction, wear and lubrication regimes ''Stribeck Curve''). We are currently developing new cermet coatings (metal matrix and ceramic reinforcement) which are deposited by different thermal spraying techniques (flame, high speed HVOF and plasma) and remelted by oxy-acetylene, flame and laser. We study the influence of different sputtering techniques on microstructure, mechanical properties and tribological behavior. On the other hand, we are developing lubricants from vegetable products as an alternative to petrochemical lubricating oils. I have belonged to the Materials Engineering research group of the Universitat Jaume I and currently I belong to the Manufacturing Processes research group of the Universitat Jaume I with code 240 through a Margarita Salas postdoctoral contract from the Ministry. I am currently doing a stay at the Institute of Materials Technology of the Polytechnic University of Valencia.

Emilio Rayón Encinas

Dr. Emilio Rayón Encinas, currently works as a senior research support technician at the Technological Institute of Materials at the Polytechnic University of Valencia, specializing in the area of materials in the following categories: Materials Science,

Physics, Polymer Science, Chemistry, Metallurgy and Metallurgical Engineering. He has collaborated in 33 projects, 54 publications in congresses, I have authored up to 55 indexed journals, I have directed 1 doctoral thesis, as in the writing of a book as participated in various scientific activities with private companies.

Julio Serrano Mira

De. Julio Serrano Mira holds a PhD in Industrial Engineering from the Universitat Jaume I and is a Professor in the Department of Industrial Systems Engineering and Design.

A member of the Manufacturing Process Engineering Department since 2004, his research has focused on intelligent manufacturing systems (especially in machining) and on the study and improvement of multi-stage manufacturing systems through the analysis of error propagation (Stream of Variation flow models).

At the teaching level, he teaches subjects such as Manufacturing Technologies, Computer Aided Manufacturing, Rapid Prototyping and Plastics Technologies.

José Vicente Abellán Nepot

José V. Abellán-Nebot holds a PhD in Industrial Engineering from the Universitat Jaume I and is a Professor in the Department of Industrial Systems Engineering and Design.

A member of the Manufacturing Process Engineering Department since 2004, his research has focused on intelligent manufacturing systems (especially in machining) and on the study and improvement of multi-stage manufacturing systems through the analysis of error propagation (Stream of Variation flow models).

During his pre- and postdoctoral training, he has spent time at prestigious research centers such as the Instituto de Estudios Superiores de Monterrey (2005), the University of Michigan (2007), the University of Arizona (2009 and 2012) and the Georgia Institute of Technology (2014).

At the teaching level, he teaches subjects such as Manufacturing Technologies, Computer Aided Manufacturing, Rapid Prototyping and Plastics Technologies.

Iván Cervera González

PhD in Engineering from the Jaume I University (Extraordinary Doctorate Award). Materials Engineer (Extraordinary Final Degree Award) and Industrial Technical Engineer from the Polytechnic University of Valencia. Master's Degree in Occupational Risk Prevention.

He joined the Jaume I University as a professor in the 2004-05 academic year in the area of Materials Science and Metallurgical Engineering.

Responsible for various subjects: Materials I and Surface Finishes (Industrial Design); Materials for Electromechanical Engineering (Industrial Engineering) and Surface Coating Techniques (Master's Degree in Science, Technology and Application of Ceramic Materials).

Assigned to the UJI Research Group "Materials Engineering", he has participated in various Research Projects, both regional and national.

His main area of research is based on Coating Technology and Thermal Spraying, with his work published in national and international journals as well as in numerous conferences.

Derived from these works, he holds two patents jointly owned with the UJI.